

# The effect of heave-face plates on FOWT heave motion: Fluid dynamic analysis

*Abdul Ghofur*<sup>1,2\*</sup>, *Aries Sulisetyono*<sup>1†</sup>, *Wibowo Harso Nugroho*<sup>2</sup>, *Baharuddin Ali*<sup>2</sup>, and *Moh. Muria Armansyah*<sup>2</sup>

<sup>1</sup>The Department of Naval Architecture, Institut Teknologi Sepuluh Nopember, Surabaya, Indonesia.

<sup>2</sup>Research Center for Hydrodynamics Technology, Research Organization for Energy and Manufacture, National Research and Innovation Agency, Sukolilo, Surabaya, Indonesia.

**Abstract.** Renewable energy technology is a topic that has often been raised in many studies lately. To support the 2020-2024 PRN (National Research Priority) program in the Maritime sector, the Researcher has developed FOWT (Floating Offshore Wind Turbine), a Classic SPAR design to operate and serve the eastern Indonesia region. A novelty design, namely the "Motion Reduction Device" (MRD), is installed at the bottom of the FOWT floater intended to increase its natural period and reduce heaving and pitching motion when exposed to environmental loads. The ANSYS FLUENT Computational Fluid Dynamics (CFD) simulation of heave decay is applied to calculate natural periods for several MRD types. A mesh convergence study was carried out to determine the best mesh size. The damping terms are derived by matching the heave motion obtained using the equation of motion by changing the damping time with linear, quadratic, or a combination of linear and quadratic. The added mass and damping results are then plotted in a graph and table. It has been demonstrated that MRD has a more significant impact than simply installing a heave plate at the bottom of the FOWT by significantly increasing added mass and damping.

## 1 Introduction

Research on PRN (National Research Priority) 2020-2024 has set 9 research focuses with superior themes that are expected to be able to make a superior product to answer the nation's strategic issues, where one of the 9 research focuses is derived from RIRN Field (National Research Master Plan), It is stated in RIRN 2017-2045 point: 4.1.8 Maritime Research Focus). Research Theme: Maritime Infrastructure Strengthening Technology; Topic: Technology development of coastal, offshore and deep water rides, Design and engineering of marine rides (surface and underwater); Target: strengthening the shipbuilding industry and supporting the domestic component industry<sup>1</sup>.

Many researchers have studied SPARs' extreme motion response and various methods for controlling the response within desired limits<sup>2</sup> found that at certain frequencies, large and

---

\* Corresponding author: [abdg001@brin.go.id](mailto:abdg001@brin.go.id); [abdulghofur68000@gmail.com](mailto:abdulghofur68000@gmail.com)

† Corresponding author: [sulisea@na.its.ac.id](mailto:sulisea@na.its.ac.id)

solid (non-perforated) heave plates have a lower heave response than perforated plates mounted on SPAR. Ezoji<sup>3</sup> looked at the heave motion of a vertical cylinder with a single heave-plate positioned on the keel. According to the results of the numerical study, extending the disk should be at least four times the normal heave amplitude to provide the best drag effect. Lin et al.<sup>4</sup> Hydrodynamic test on four types of SPAR models to understand the effect of adding heave devices on motion response characteristics. The positive effect of "strake plate" and "heave plate" on damping has been confirmed. Chakrabarti<sup>5</sup> conducted wave resonance measurements on a semisubmersible truss-pontoon model equipped with a heave plate to better understand the damping influence on heave and pitch responses. The damping flow separation caused by the heave plates near resonance is roughly five times more than free-decay damping for heave and nine times greater for pitch; these values will restrict the peak amplitudes of heave and pitch. Tao<sup>6</sup> investigated the effect of "span-wise length"  $L/Dd$  ( $L$  distance between heave-plates and  $Dd$ -heave-plate diameter) on hydrodynamic properties such as added-mass and damping coefficients on a vertical cylinder with two heave-plates using a finite difference approach. According to the findings, the damping ratio rises with increasing spanwise length due to the significant interaction between distinct heave-plate vortices, up to a critical limit of relative distance ( $L/Dd$ ). Tao and Dray<sup>7</sup> investigated the hydrodynamic characteristics of oscillating solid and porous heave plates by conducting scale model tests. A heave plate with a porosity of 20% produces an increase in damping of around 30% compared to a solid one at  $f=0.1\text{Hz}$  and  $KC=0.2$ . From the literature, it can be concluded that the effectiveness of the heave plate in reducing the resonant heave response of the SPAR system depends on the diameter span-wise length ratio ( $Dd/Dc$ ). Hydrodynamic coefficients for excitation forces, added mass, damping, and hydrostatic restoration can be solved in the frequency domain or time domain. In order to solve time-domain equations, the results of the frequency domain may be used to obtain time-domain coefficients. Sudhakar et al.<sup>8</sup> investigated the effects of moon-pool, strake, and heave plate on the generation of heave and pitch from various SPAR configurations at a scale of 1:400. It has been demonstrated that spiral strake and heave plate are effective in reducing resonance period by 25% to 50%.

Floating Offshore Wind Turbine (FOWT) type semi-submersible has been researched by Amaral<sup>9</sup>, where he has carried out the FOWT model testing by observing the dynamic coupling response. A conventional catenary mooring system is used to anchor the model. The incoming wave and wind excitation are generated un-unidirectional. The results obtained are that the response coupling effect shows a high response that is quite significant, especially the pitch motion. He informs the next researchers, who carry out FOWT testing with floaters, not to simplify model testing, especially where all loads are colinear (wind, wave and current in the same direction). Nguyen<sup>10</sup> Compare several floater types of FOWT, i.e., Barge, TLP and SPAR, which involve operating conditions, property and applicability. The SPAR-Floating Offshore Wind Turbine (S-FOWT) have advantages in deep water, such as a small water line area with little volume close to the free surface, resulting in small wave forces. Catenary mooring is inexpensive and simple to set up. Platform geometry that is easy to fabricate, low maintenance, simple to operate, and has a long natural period. It is also stable in wind and wave loads.

For all of the above research, the use of heave plates could still be optimized in terms of reducing heave amplitude and increasing the natural period. It is now proposed a new novelty design known as a Motion Reduction Device (MRD) is similar to a face plate wrapped around the outer side of a heave plate, with the assumption that the installed MRD traps some volume of water, increasing added mass and damping. To demonstrate this, the fluid is considered to be viscous in order to produce a reasonably realistic turbulent effect. ANSYS FLUENT, a computational fluid dynamics (CFD) program, is utilized with the k-omega SST (Shear-Stress Transport) turbulent model equation.

The FOWT 500kW within a medium-sized (17-meter draft) SPAR-type structure is simple, easy, efficient, and practical. It is in high demand for people who live in coastal areas far from state power sources. It is therefore recommended to install an MRD on a medium-sized SPAR to significantly reduce the heave motion of the FOWT, allowing the FOWT to operate effectively in shallow and moderate water depths. It is very much in demand for people who live in coastal areas far from state electricity sources.

## 2 Design FOWT

Compare the operating conditions, property, and applicability of various floater types of FOWT: barge, semisubmersible, TLP, and SPAR. The FOWT type SPAR has advantages for deep-water operation, such as a small water line area with a small volume close to the free surface, which results in low wave forces. Nguyen<sup>10</sup> Catenary mooring is inexpensive and easy to install. Platform geometry that is simple to build and maintain, has a long natural period, and is easy to operate. It is also resistant to wind and wave loads. Many studies of FOWTs have been conducted recently experimentally using scale model<sup>11,12,13</sup>, the SPAR drafts ranging from 50 to 80 meters. Using in-house software, Liang Tian<sup>14</sup> demonstrated FOWT motion analysis. From his simulation, he concluded that surge and pitch were dominant motions. According to the aforementioned literature studies, there are still few studies that evaluate the effect of heave plate presence on FOWT and its effect on damping and added mass.

Karimirad<sup>15</sup> has introduced a Short-SPAR type wind turbine suitable for moderate water depth. It is a catenary-moored SPAR-type wind turbine, and an appropriate design was discovered at a lower depth. In the SPAR concept, the capital cost and displacement volume (total mass) are inextricably linked. The goal is to have a small displacement volume. Although the overall mass of the Short-SPAR (structural mass + ballast) is 35% less than that of the Deep-SPAR, the statistical properties of the produced power are nearly identical for both spars. Short-SPAR mass reduction contributes to a more cost-effective option for floating wind turbines in moderate water depths.

**Table 2.1.** Main dimension FOWT.

MAIN DIMENSION FOWT (FLOATING OFFSHORE WIND TURBINE)

SCALE : 20

Description	Symbol		Fullscale		Model scale
Height of Floater	H	=	25.00 m		1.25 m
Diameter of Hull	B	=	4.00 m		0.20 m
Draft	T	=	17.00 m		0.85 m
Displacement	Disp	=	218,969.01 kg		26.7035 kg
Long. Center of Gravity from AP	LCG	=	2.00 m		0.10 m
Center of Gravity from keel	KG	=	7.59 m		0.3795 m
Vertical Center of Bouyancy	KB	=	8.50 m		0.4250 m
BM trans	BMt	=	34.30 m		1.715 m
BM long	BMI	=	34.30 m		1.715 m
Kxx	(approx.)	=	1.10 m		0.055 m
KMt (from Carene calculation)		=	42.80 m		2.14 m
GMt		=	35.21 m		1.7605 m



**Figure 2.1.** Drawing FOWT

A parametric study for the selection of geometric main dimensions and weight are conducted with several constraints including: water depth, dimensions, blade diameter (300 kW capacity) and weight distribution of the upper structure (blade, nacelle, tower and batteries). Result of the FOWT 300 kW main dimension is provided (see Table 2.1). The heave plate design is variable, with diameters ranging from 5.4m to 6.0m and 8.0m (full scale) and heave face plate height of 1 m (full scale) see Figure 2.2 and Table 2.2.

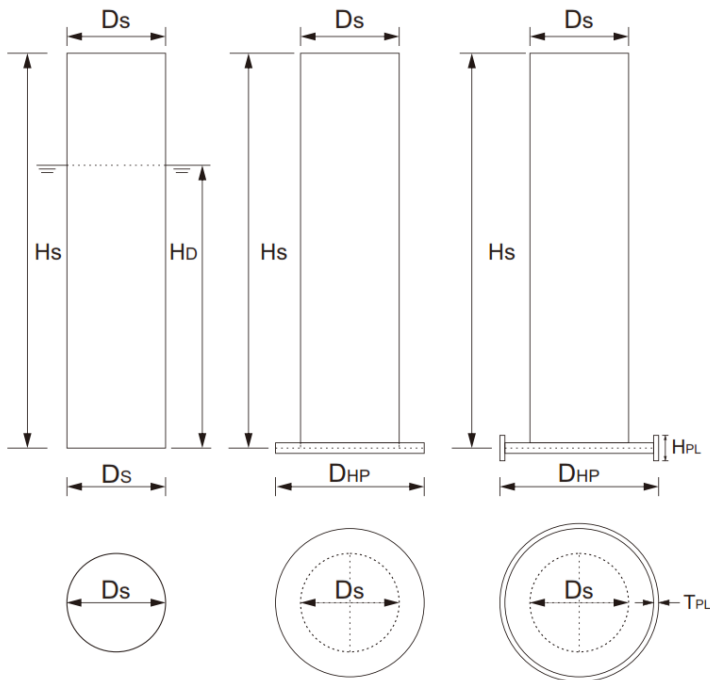


**Figure 2.2.** Dimension FOWT

**Table 2. 2.** Heave-Plate and Heave-face plate dimension

Description	Symbol	Type A	Type B	Type C	Type D	Unit
Diameter of SPAR	Ds	4.00	4.00	4.00	4.00	M
Total height of SPAR	Hs	25.00	25.00	25.00	25.00	M
Draft	Hd	17.00	17.00	17.00	17.00	M
Diameter of Heave Plate	Dhp	0.00	5.20	6.40	8.00	M
Diameter Ratio (Dr)	Dhp/Ds	1.00	1.30	1.60	2.00	-
Height of Heave-face plate	Hpl	1.00	1.00	1.00	1.00	M
Thickness of Heave Plate	Tpl	0.15	0.15	0.15	0.15	M

### 3 Method

The methodology used in this study is described in the following order:

- Data on Classic SPAR type FOWTs that have been built, as well as research results, were obtained through a literature review.
- Design SPAR main dimensions within constraints (water depth, 300 kW Wind Turbine capacity, and upper structure weight).
- Determine the main dimension and inertial characteristics of the FOWT (L, B, T, Displacement, KG, GM, Radius of gyration).
- Create a heave plate with a variety of heave plate diameter/SPAR diameter (Dh/Ds) ratios. As well as a heave-face plate.
- Numerical modeling: Geometry model using Solid Work Body FOWT (Classic-SPAR body, heave plate, and heave-plate let for all specified variations).
- Numerical Analysis: Set-up and Solution. Includes General, Boundary conditions, Solution, Initialization, number of time steps and iterations. Output: added mass, displacement vs time and fluid velocity plot around the heave plate.
- Conduct analytical calculations to determine heave damping and heave added mass values. Tabulated and plot all the results.
- Analysis, discuss the results and draw conclusions.

### 4 Numerical Simulation

CFD simulations of free heave decay of SPAR (no-heave plate, with heave plate and with heave-face plate) were performed in a numerical tank of dimensions: length 4000 mm, breadth 1200 mm and height 1750 mm within water depth of 1150 mm. The SPAR geometry is modelled with initial heave displacement inside the numerical tank with the x-y plane as water plane. Meshing operation of numerical domain was performed using meshing software, ANSYS FLUENT. The meshing zones of 3D numerical tank are shown in schematic diagram (Figure 4.1). Structured mesh with circularly arranged hexahedral mesh is used in the inner region (of radius of 480 mm) and undistorted hexahedral mesh is used in the outer region. The inner and outer regions are fused by a transitional mesh. Reynolds Averaged Navier Stokes equation (RANS) was solved inside the numerical domain using a finite volume CFD solver ANSYS FLUENT to obtain velocity and pressure.

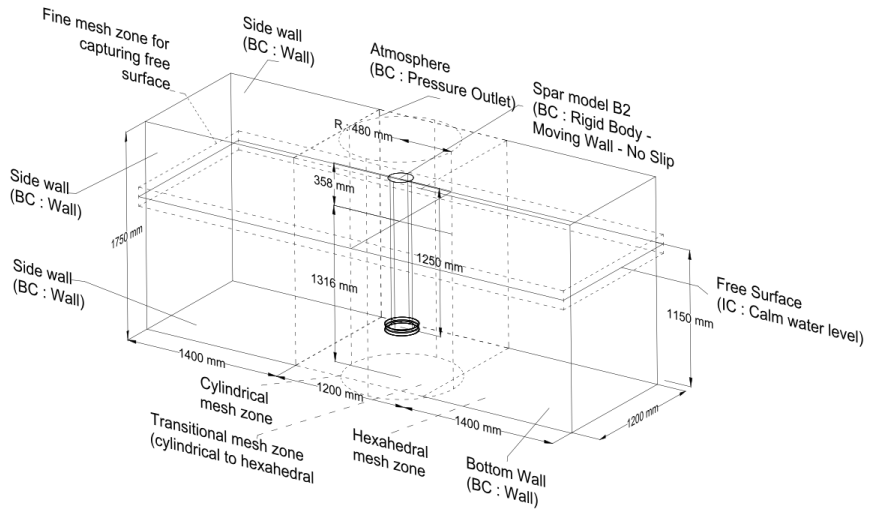


**Figure 4.1** 3D numerical simulation domain tank

Table 2.1 shows the spar model main dimension properties such as displacement, center of gravity (COG), and mass moment of inertia that are threatened as input to the solver via a user defined function (UDF). At each time step, the position of the floating body is updated using the dynamic mesh update method. The heave displacement is calculated by taking an area weighted average of the z-coordinates of each face element on the spar model's surface. Table 4.1 displays the number of geometry variations of the running program in the numerical analysis.

**Table 4.1.** Model Geometry Variations of the running program.

Type	D <sub>S</sub> (mm)	D <sub>HP</sub> (mm)	H <sub>PL</sub> (mm)
A	200	-	-
B1	200	260	-
B2	200	260	50
C1	200	320	-
C2	200	320	50
D1	200	400	-
D2	200	400	50

#### 4.1 Mesh generation and Meshing convergence test

Figure 4.2.a and Figure 4.2.b show how a finer zone mesh was used near the water level to accurately capture the free surface. For the spar with heave plate, the mesh size was varied from 35 mm to 15 mm along the depth direction and radial direction.

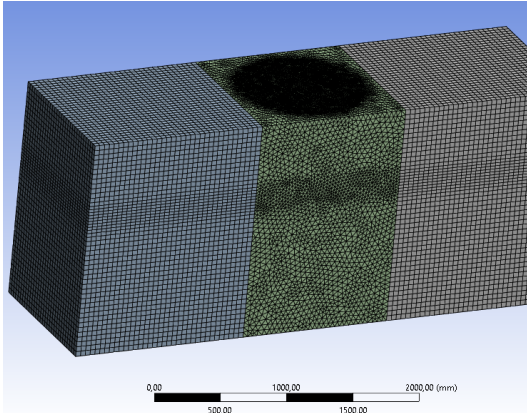


**Figure 4.2.a** CFD meshing results

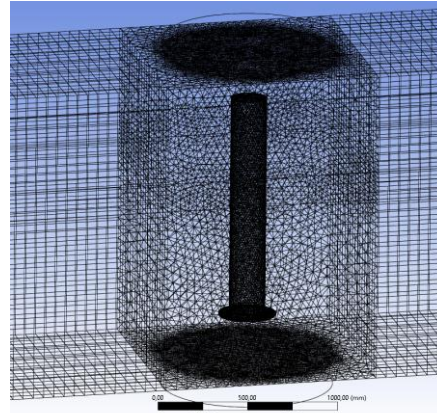


**Figure 4.2.b** Meshing SPAR in the computational domain

The spar models experienced 35 mm initial heave displacements. Figure 5.2 shows the heave response resulting from CFD simulation of free decay. The converged mesh grid independence study information was used to vary the mesh size in the radial direction after obtaining mesh size convergence in the normal direction. Convergence tests are carried out to guarantee that the number of elements has no influence on meshing quality. In each meshing experiment, the number of elements is varied.

**Table 4.2.** Grid Independence Simulation of Damping coefficient.

Number of Cells	Damping (B1)	Percentage
514,318	0.39	-
1,115,729	0.55	42.59
1,950,507	0.56	0.14
3,503,832	0.56	0.09

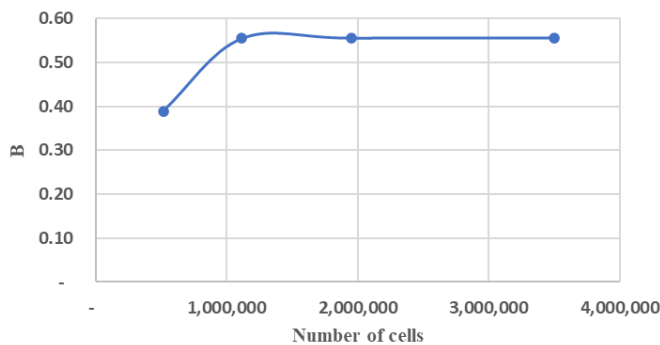


**Figure 4.3.** Grid Independence Simulation of Damping coefficient

The output of this simulation is heave displacement vs time. The damping coefficient is then determined by changing the heave displacement graph. The simulation is repeated for a new number of cells, which is usually around double the number of prior simulations. The information is then tabulated (see Table 4.2). If the difference in damping coefficient values

is less than 2%, the number of cells is regarded good<sup>16</sup>. This study simulates with damping coefficient values varying by less than 1%.

## 4.2 Numerical analysis set up

As a computational domain shown in Figure 2. The boundary condition is taken as a no-slip wall element with the fluid flow is Mesh generation. In FEM based CFD method, any type of element is adequate to perform meshing activity. However, it is claimed that the linear tetrahedral element has performed better solution<sup>10</sup>. A mathematic equation model of RANS was applied to the analysis and the equation is written in Equation (1)<sup>17</sup>.

$$\rho \frac{\partial U_i}{\partial t} + \rho U_i \frac{\partial U_i}{\partial x_j} = -\frac{\partial P}{\partial x_i} + \frac{\partial}{\partial x_j} \left( 2\mu s_{ij} - \overline{\rho u_j u_i} \right) \quad (1)$$

The k- $\omega$  SST model, which is widely used to represent turbulence models, was utilized as a well-established way to provide closure to the RANS equations<sup>18, 19</sup>. Equations (2) and (3) express the turbulence kinetic energy and specific dissipation rate of the k- $\omega$  SST turbulence model<sup>18</sup>.

$$\frac{\partial k}{\partial t} + U_j \frac{\partial k}{\partial x_j} = P_k - \beta^* k \omega + \frac{\partial}{\partial x_i} \left[ (v + \sigma_k v_T) \frac{\partial k}{\partial x_j} \right] \quad (2)$$

$$\frac{\partial \omega}{\partial t} + U_j \frac{\partial \omega}{\partial x_j} = \alpha S^2 - \beta \omega^2 + \frac{\partial}{\partial x_i} \left[ (v + \sigma_\omega v_T) \frac{\partial \omega}{\partial x_j} \right] + 2(1 - F_1) \sigma \omega^2 \frac{1}{\omega} \frac{\partial}{\partial x_i} \frac{\partial \omega}{\partial x_i} \quad (3)$$

The k- $\omega$  SST Is a combination of k- $\epsilon$  (for flow distant from the boundary layer) and k- $\omega$  (for flow within the boundary layer). Furthermore, in k- $\epsilon$  models, the k stands for turbulent kinetic energy and  $\epsilon$  represents dissipation energy, respectively, as indicated in Equation (4) and Equation (5).

$$\frac{\partial}{\partial t} (\rho k) + \frac{\partial}{\partial x_i} (\rho k u_i) = \frac{\partial}{\partial x_j} \left[ \left( \mu + \frac{\mu_t}{\sigma_k} \right) \frac{\partial k}{\partial x_j} \right] + P_k + P_b - \rho \epsilon - Y_M + S_k \quad (4)$$

$$\frac{\partial}{\partial t} (\rho \epsilon) + \frac{\partial}{\partial x_i} (\rho \epsilon u_i) = \frac{\partial}{\partial x_j} \left[ \left( \mu + \frac{\mu_t}{\sigma_\epsilon} \right) \frac{\partial \epsilon}{\partial x_j} \right] + C_{1\epsilon} \frac{\epsilon}{k} (P_k + C_{3\epsilon} P_b) - C_{2\epsilon} \rho \frac{\epsilon^2}{k} + S_\epsilon \quad (5)$$

## 4.3 CFD analysis result

The decay motion in heave direction is the results of CFD, and then it plots for each type of heave plate (A to D) as can be shown in Figure 4.6 to 4.8. Turbulent flow is observed at the end of the heave plate for cylinder with heave plates (B1, C1, and D1). Turbulence is apparent in the upper and lower parts of the face plate for heave plates complete with face plates (B2, C2, and D2) see figure 4.4. This demonstrates that the faceplate retains the fluid and that part of it flows out to generate turbulence at both ends of the faceplate.

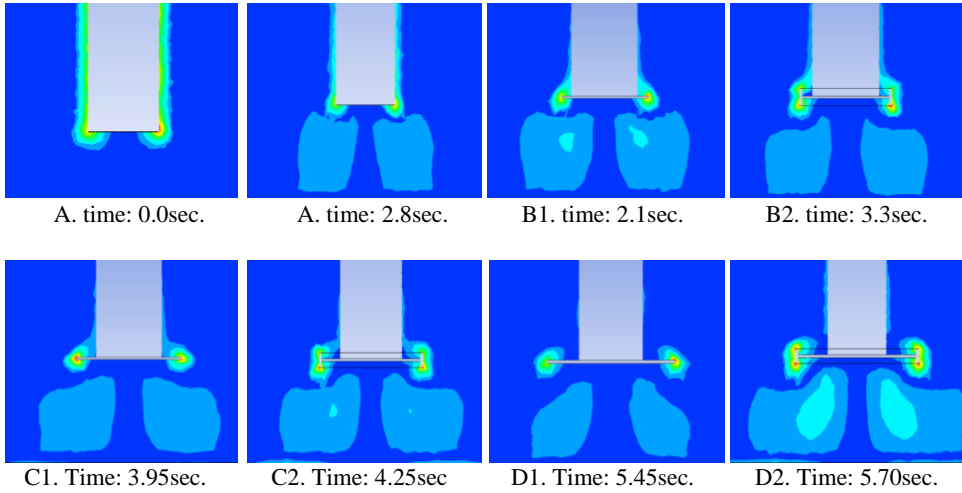


**Figure 4.4.** Plot result velocity curl during decay in heave direction (SPAR type A to type D)

Following the graphical representation of time-traces plot (displacement versus time), next step is to do a damping analysis using the following mathematical method. In the analysis decay, data in form of time traces, a mode of motion is defined as in the example in Figure 4.5.

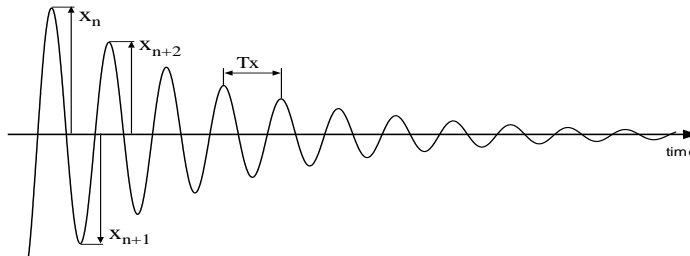


**Figure 4.5.** Time trace decay motion

The decrease in motion amplitude in decay  $x$  is defined as a polynomial function of average amplitude  $x_m$  and is written as follows:

$$\Delta x = ax_m + bx_m^2 \tag{6}$$

Or in the form of Bertin's coefficient  $N$ , the amplitude reduction of  $x$  is described as a function of mean square amplitude  $x_m^2$  as follows:

$$\Delta x = Nx_m^2 \tag{7}$$

then from equations (6) and (7) are could be found  $N$ :

$$N = a/x_m + b \tag{8}$$

Where the values of  $a$  and  $b$  may be calculated using the least square approach and plotted in the function  $(x_m, \Delta x)$  extinction curve, where where  $\Delta x = |x_{n+1} - x_n|$  and  $x_m = |(x_{n+1} + x_n)/2|$ .

The most often used equation of motion in free decay, which merely employs linear damping  $B_1$ . Where  $B_1$  is the motion of a floating item in still water, which may be considered to be as follows:

$$(M + \Delta M) \frac{d^2x}{dt} + B_1 \frac{dx}{dt} + kx = 0 \tag{9}$$

Some references <sup>5</sup> show that the equation of motion of a floating object by including non-linear damping components  $B_2$  will show better results, then the equation of motion for free decay can be written as follows:

$$(M + \Delta M) \frac{d^2x}{dt} + B_1 \frac{dx}{dt} + B_2 \frac{dx}{dt} \left| \frac{dx}{dt} \right| + kx = 0 \tag{10}$$

Where  $(M + \Delta M)$  mass and added mass for translational motion (for rotational motion mode becomes  $(I + \Delta I)$  inertia and added inertia moment),  $B_1$  and  $B_2$  are linear and quadratic motion damping, respectively, and  $k$  is the restoring moment. The dissipating energy in motion decay for each half roll period ( $T/2$ ), which was explained by Ali<sup>20</sup>, is integral to equation (10). If the following is assumed:

$$x = A \cos \omega t \tag{11}$$

so :

$$\int_0^{T/2} \left( (M + \Delta M) \frac{d^2x}{dt} \right) \frac{dx}{dt} dt = 0 \tag{12}$$

$$\int_0^{T/2} \left( B_1 \frac{dx}{dt} \right) \frac{dx}{dt} dt = B_1 \frac{\pi^2}{T} x'^2 \tag{13}$$

$$\int_0^{T/2} \left( B_2 \frac{dx}{dt} \left| \frac{dx}{dt} \right| \right) \frac{dx}{dt} dt = B_2 \frac{16\pi^2}{3T^2} x'^3 \tag{14}$$

$$\int_0^{T/2} kx \frac{dx}{dt} dt = -kx' \Delta x \tag{15}$$

From equation (13) ~ (15) are found:

$$B_1 \frac{\pi^2}{T} x'^2 + B_2 \frac{16}{3T^2} x'^3 - kx' \Delta x = 0 \tag{16}$$

$$\Delta x = \frac{1}{k} \left( B_1 \frac{\pi^2}{T} \right) x' + \frac{1}{k} \left( B_2 \frac{16\pi^2}{3T^2} \right) x'^2 \tag{17}$$

Equation (17) can be linearized similar to equation (1). If  $x' = x_m$  then the coefficient values  $a$  and  $b$  are obtained in the decrement motion decay equation in equation (6) respectively:

$$a = \frac{1}{k} \left( B_1 \frac{\pi^2}{T} \right) \quad \text{and} \quad b = \frac{1}{k} \left( B_2 \frac{16\pi^2}{3T^2} \right) \tag{18}$$

if it is known that  $k = \omega^2 m$ , where  $m = (M + \Delta M)$  then (18) can be written as in (19):

$$B_1 = \frac{4}{T} a \quad \text{and} \quad B_2 = \frac{3}{4} b m \tag{19}$$

The magnitudes of the linear and quadratic damping coefficients in that mode of motion are indicated by the values of  $a$  and  $b$ . The decay test may be used to determine the values of  $B_1$  and  $B_2$  based on these coefficients.

A curve of extinction was produced using the values of  $\Delta x$  and  $x_m$  using the measurement results of the maxima-minima values in the decay test. The values of  $a$  and  $b$  in equation (6) will be derived by utilizing the *least square method*. The appearance of the value of motion damping in *N Bertin's Coefficient* by applying the  $a$  and  $b$  values of equation (8). Furthermore, linear and quadratic damping values ( $B_1$  and  $B_2$ ) will be calculated from equation (19) and used to calculate decay motion as in equation (10).

### Natural Period and Damping

Figures 4.6 to 4.8 show time traces of heave motion decay FOWT for each type of heave plates, allowing the natural period and damping to be determined.

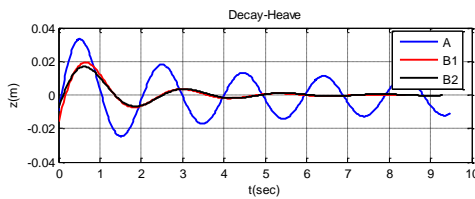


**Figure 4.6.a.**

Time traces heave decay type A and B

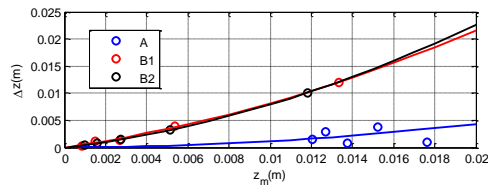


**Figure 4.6.b**

Extinction curve heave decay type A and B

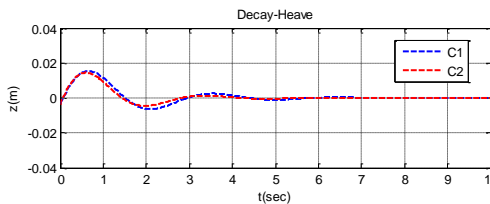


**Figure 4.7.a**

Time traces heave decay type C

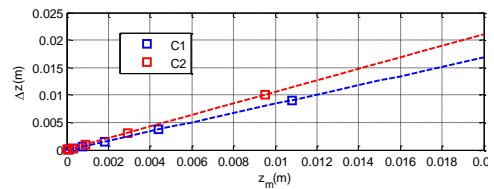


**Figure 4.7.b**

Extinction curve heave decay type C

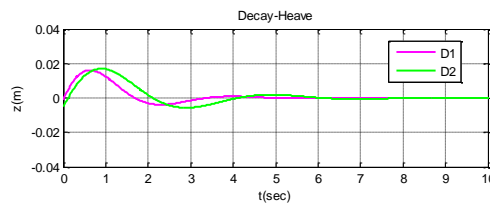


**Figure 4.8.a**

Time traces heave decay type D

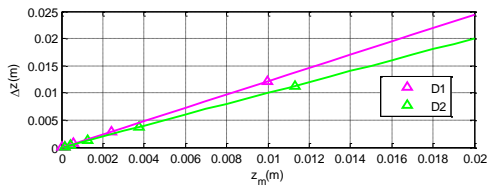


**Figure 4.8.b**

Extinction curve heave decay type D

The Natural period and Damping coefficient of each heaving plate type are given below based on the CFD output:

**Table 4.3** Natural period

Type	Tn (sec.)	Diff. (%)
A	1.9593	0.00
B1	2.3556	20.23
B2	2.3730	21.11
C1	2.7853	42.16
C2	2.8526	45.59
D1	3.3409	70.51
D2	3.9979	104.05

**Table 4.4** Quadratic damping Coefficient

Type	a	b
A	10.0698	0.0141
B1	26.1159	0.5548
B2	33.8602	0.4536
C1	0.0024	0.8393
C2	0.0072	1.0525
D1	0.0257	1.2214
D2	0.0033	1.0006

The differences (%) of SPAR natural period with heave plates (types B, C, and D) compared to without heave plates (type A) are calculated by using equation (20), as shown in table 4.3. The quadratic damping coefficients formulated in equation (6) are tabulated on table 4.4.

$$Diff = \frac{T_{type} - T_A}{T_A} \times 100\% \quad (20)$$

Tables 4.3 and 4.4 indicate that heave damping and natural period increase as the diameter ratio increases. Heave damping rises as vorticity increases around the heave plate. Because damping and added mass rise, so does the heave natural period. It rose by 20%, 42%, and 70% for types B1, C1, and D1 (with heave plate) compared to type A (without heave plate).

Next, the effect of face plate is also quite clear, increasing the natural heave period by 1% (B2>B1) and 3% (C2>C1), respectively, but it increases dramatically by 19.6% (D2>D1). This may be explained as follows: vorticity at both ends of the face plate as the cylinder travels up and down, followed by a number of fluid volumes trapped in the gap between the cylinder and the face plate, increasing the inertia of the SPAR body.

#### Added Mass

For a SPAR without heave plate, Newman<sup>21</sup> has estimated the heave added mass ( $A_{33}$ ) of an semi-infinite cylinder floating in water as write in equation (21):

$$A_{33} = (2/3)\rho\pi R_s^3 \quad \text{or} \quad A_{33} = 2.0944\rho R_s^3 \quad (21)$$

Where  $A_{33}$  is heave added mass,  $\rho$  is mass density,  $R_s$  is SPAR cylinder radius.

For SPAR with heave plate (type B, C and D), added mass has been proposed by Philip<sup>22</sup> based on geometric shape of a SPAR with a heave plate attached to the bottom of the cylinder as can be seen in equation (22)

$$A_{33} = \frac{1}{3}\rho D_{hp}^3 - \frac{1}{6}\rho \left[ D_{hp}^3 - (D_{hp}^2 - D_s^2)\sqrt{D_{hp}^2 - D_s^2} \right] \quad (22)$$

Added mass ( $A_{33}$ ) calculations were also performed using NEMOH v.3.0<sup>23</sup>. It is a Boundary element Methods (BEM) algorithm for calculating wave loads on offshore structures such as: added mass, radiation, damping, and diffraction forces.

**Table 4.5** Heave added mass ( $A_{33}$ )

Type	$D_{HP}/D_S$ (m)	NEMOH (kg)	Theoretical (kg)	Diff (%)
A	1.0	2.1505	2.0944	2.68
B1	1.3	3.8219	3.6935	3.48
B2	1.3	4.9405	3.6935	33.76
C1	1.6	13.0519	8.0593	61.95
C2	1.6	15.1421	8.0593	87.88
D1	2.0	20.2854	17.5949	15.29
D2	2.0	42.6758	17.5949	142.55

Table 4.5 shows NEMOH and Theoretical numerical calculations for the  $D_{HP}/D_S$  ratio = 1.3 demonstrate that it increases added mass ( $A_{33}$ ) by around 77%. Sudhakar<sup>8</sup> also showed that with the same diameter ratio 1.3, ( $A_{33}$ ) increases by almost 75%. It is also demonstrated that the inclusion of a face plate raises  $A_{33}$  by 110% ( $D2>D1$ ) compared to merely employing a heave plate.

Meanwhile, for those employing face plates (B2, C2, and D2), the numerical results differ significantly from manual (theoretical) calculations, because manual calculations do not incorporate face plate parts. Whereas for types  $B2/B1=1.29$ ,  $C2/C1=1.16$ , and  $D2/D1=2.10$ , the inclusion of a face plate increases considerably added mass.

## 5 Conclusion

SPAR Classic FOWT with 25m length and 4m diameter. A heave plate with diameter ratios of 1.0, 1.3, 1.6, and 2.0 is added to the bottom. A one-meter-high face plate perpendicular to the end of the heave plate was also installed. After doing Computational Fluid Dynamics (CFD) at a scale of 1:20. The following are some conclusions:

- As predicted, the output plot confirms earlier study findings that the usage of heave plates improves added mass, damping, and natural period.
- The use of a Heave plate increases the natural heave period by 20%, 42%, and 70% for types B1, C1, and D1 (with heave plate) compared to type A (without heave plate).
- The installation of a face plate gives greater benefit than just placing a heave plate; it raises the natural heave period by 1% ( $B2>B1$ ) and 3% ( $C2>C1$ ), respectively, but by 19.6% ( $D2>D1$ ).
- Application of heave plate ratio ( $D_{HP}/D_S$ ) = 1.3 demonstrate that it increases added mass ( $A_{33}$ ) by around 77%. It is also demonstrated that the inclusion of a face plate raises  $A_{33}$  by 110% ( $D2>D1$ ) compared to merely employing a heave plate.
- Future work. Hydrodynamic model testing, including decay tests and wave tests, will be carried out using the same model size of 1:20. To offer a comprehensive picture of the functioning of the MRD placed on the SPAR Classic type FOWT for operating at water depths ranging from 25 to 60 meters.

The author is grateful to the Republic of Indonesia's National Research and Innovation Agency (BRIN) for sponsoring this research and so many thanks to The Department of Naval Architecture Institut Teknologi Sepuluh Nopember Indonesia for supporting the research.. The author would also like to thank the promotor, co-promotor, and colleagues for their guidance, helps and encouragement, as well as technical personnel or other support from the Research Center for Hydrodynamics Technology in Surabaya, Indonesia.

## References

1. Ristekdikti. *Rencana Induk Riset Nasional Tahun 2017-2045*. (2017).
2. Downie, M. J., Graham, J. M. R., Hall, C., Incecik, A. & Nygaard, I. An experimental investigation of motion control devices for truss spars. *Mar. Struct.* **13**, 75–90 (2000).
3. Ezoji, M., Shabakhty, N. & Tao, L. Hydrodynamic damping of solid and perforated heave plates oscillating at low KC number based on experimental data: A review. *Ocean Eng.* **253**, 111247 (2022).
4. Lin, C. L., Tawhai, M., McLennan, G. & Hoffman, E. *Computational fluid dynamics*. *IEEE Engineering in Medicine and Biology Magazine* vol. 28 (2009).
5. Chakrabarti, S. K. *Handbook of Offshore Engineering*. *Handbook of Offshore Engineering* vol. I (Elsevier Ltd, 2005).
6. Tao, L., Molin, B., Scolan, Y. M. & Thiagarajan, K. Spacing effects on hydrodynamics of heave plates on offshore structures. *J. Fluids Struct.* **23**, 1119–1136 (2007).
7. Tao, L. & Dray, D. Hydrodynamic performance of solid and porous heave plates. *Ocean Eng.* **35**, 1006–1014 (2008).
8. Sudhakar, S. INFLUENCE OF HEAVE PLATE ON HYDRODYNAMIC RESPONSE OF SPAR. in *Proceedings of the ASME 2011 30th International Conference on Ocean, Offshore and Arctic Engineering OMAE2011* (OMAE, 2011). doi:<https://doi.org/10.1115/OMAE2011-49565>.
9. Amaral, G. A. *et al.* Seakeeping tests of a fowt in wind and waves: An analysis of dynamic coupling effects and their impact on the predictions of pitch motion response. *J. Mar. Sci. Eng.* **9**, 1–19 (2021).
10. Dinh, V. N. & Basu, B. On the modeling of spar-type floating offshore wind turbines. *Key Eng. Mater.* **569–570**, 636–643 (2013).
11. Wen, T. R., Wang, K., Cheng, Z. & Ong, M. C. Spar-type vertical-axis wind turbines in moderate water depth: A feasibility study. *Energies* **11**, (2018).
12. Utsunomiya, T. *et al.* At sea experiment of a hybrid spar for floating offshore wind turbine using 1/10-scale model. *J. Offshore Mech. Arct. Eng.* **135**, 34503-1-34503–8 (2013).
13. Jiang, Z. *et al.* Feasibility studies of a novel spar-type floating wind turbine for moderate water depths: Hydrodynamic perspective with model test. *Ocean Eng.* **233**, 109070 (2021).
14. Tian, X. liang, Xiao, J. ren, Liu, H. xue, Wen, B. rong & Peng, Z. ke. A Novel Dynamics Analysis Method for Spar-Type Floating Offshore Wind Turbine. *China Ocean Eng.* **34**, 99–109 (2020).
15. Karimirad, M. & Moan, T. Feasibility of the application of a spar-type wind turbine at a moderate water depth. *Energy Procedia* **24**, 340–350 (2012).
16. Molland, A. F. & Utama, I. K. A. P. Experimental and numerical investigations into the drag characteristics of a pair of ellipsoids in close proximity. *Proc. Inst. Mech. Eng. Part M J. Eng. Marit. Environ.* **216**, 107–115 (2002).
17. Launder, B. E. First steps in modelling turbulence and its origins: A commentary on Reynolds (1895) ‘On the dynamical theory of incompressible viscous fluids and the determination of the criterion’. *Philos. Trans. R. Soc. A Math. Phys. Eng. Sci.* **373**, (2015).

18. de Sousa, J. V. N. *et al.* *On the Study of Autonomous Underwater Vehicles by Computational Fluid-Dynamics*. *Open Journal of Fluid Dynamics* vol. 10 (2020).
19. Ghofur, A., Arifin, Arianti, E., Bisri, A. & Suwahyu. Resistance on Catamaran Decommissioning Unit: A Comparison of Numerical Analysis (Two Turbulence Models) to Model Test Result. *IOP Conf. Ser. Earth Environ. Sci.* **1166**, (2023).
20. Murdjito *et al.* Experimental study on heave damping due to the heave plate addition on the SPAR keel. *IOP Conf. Ser. Earth Environ. Sci.* **649**, (2021).
21. Newman, J. N. *Marine Hydrodynamics*. (The MIT Press Cambridge, Massachusetts London, England).
22. Nallayarasu, S. Omae2012-83290. 1–12 (2017).
23. Ducrozet, R. K. and G. *NEMOH v3.0 User Manual*. (2022).